MATERIALS PHYSICS AND MECHANICS RESEARCH ARTICLE

Submitted: September 26, 2025 **Revised: November 1, 2025** **Accepted: November 14, 2025**

The design of Zn_2SiO_4 pigments for thermal control coatings

M.M. Mikhailov [1], A.V. Filimonov [2], A.N. Lapin [1], S.A. Yuryev [1] ✉, V.A. Goronchko [1], D.S. Phedosov [1]

[1] Tomsk State University of Control Systems and Radioelectronics, Tomsk, Russia

[2] Peter the Great St. Petersburg Polytechnic University, St. Petersburg, Russia

✉ yusalek@gmail.com

ABSTRACT

Zn_2SiO_4 pigments were synthesized from ZnO and SiO_2 powders obtained from different manufacturers at various concentration ratios and differing in particle size and specific surface area. The optimal values of particle size and specific surface area were determined, thus making it possible to obtain the pigments with a small value of solar absorptance (α_s). The α_s values of the synthesized pigments were compared with other types of pigments used to design thermal control coatings. The study showed that it is possible to synthesize Zn_2SiO_4 powders with high reflectivity in a wide spectral range (200–2500 nm) and a small value of solar absorptance (α_s = 0.077) - significantly lower compared to ZnO powders - using a solid-state method from zinc oxide micropowders and silicon dioxide nanopowders.

KEYWORDS

thermal control coatings • pigments • synthesis • diffuse reflectance spectra • solar absorptance

Funding. *The work was carried out with the financial support of the Ministry of Science and Higher Education of the Russian Federation (Goszadanie No. FEWM-2023-0012).*

Citation: Mikhailov MM, Filimonov AV, Lapin A.N, Yuryev SA, Goronchko VA, Phedosov DS. The design of Zn_2SiO_4 pigments for thermal control coatings. *Materials Physics and Mechanics*. 2025;53(5): 74–82. http://dx.doi.org/10.18149/MPM.5352025_5

Introduction

The temperature of space objects is maintained at a given level by thermal control systems, which include active and passive components [1,2]. The active component is composed of cooling gases, pumps, gas pipelines, and check valves. It is activated in emergencies upon temperature rising [3]. As for the passive thermal control component, it plays the main role in maintaining the temperature at a certain level. It takes the form of a coating applied to thermal control radiators, housings, and individual devices. This coating operates throughout the entire period of orbital flights. Thermal control coatings (TCC) reflect the electromagnetic radiation of the Sun and re-emits the heat generated during the operation of the on-board equipment. The temperature of the objects is solely determined by the absorption of solar energy and by the re-emission of heat released by the on-board equipment. According to the Stefan–Boltzmann law, it can be determined via the following expression: $T \sim k \cdot (\alpha_s/\varepsilon)^{1/4}$, where k is the coefficient comprising the areas of absorbing and emitting surfaces, α_s is the value of solar absorptance, ε is the emissivity of TCC.

If other conditions are kept equal, the temperature is considered proportional to α_s absorption coefficient. Therefore, it is necessary to reduce the value of α_s in order to decrease the area of both TCC and thermal control radiators and to maintain the required temperature. According to international standards [4,5], the values of absorptance should

fall within $\alpha_s \leqslant 0.2$ for TCCs of the optical solar reflector (OSR) class. This requirement is met for the existing conventional TCCs. However, it is necessary to design the coatings with lower α_s values in order to reduce their area, weight, and cost. The TCCs based on dielectric and semiconductor pigments with α_s varying from 0.12 to 0.15 are currently used in thermal control systems [6–8]. To design TCCs with even lower absorption coefficient values, various combinations of components have been recently used in the pigment design. The usage of these components allows one to obtain $\alpha_s \leqslant 0.1$.

The second requirement for modern OSR TCCs is the high stability of absorption coefficient under operating conditions. A number of methods have been recently developed to increase the radiation stability of TCCs, their pigments and binders when they are exposed to solar spectrum quanta and charged particles. These methods are mainly based on three principles:

1. on the modification of TCCs by nanoparticles that act as small-size relaxation centers for primary photo- and radiation defects caused by irradiation;
2. on the modification of TCCs by rare earth elements (REE) that absorb the primary radiation-induced defects;
3. on the formation of protective layers with higher radiation stability on the surface of TCCs. If the composition of TCC includes nanoparticles or SiO_2 particles, which form protective layers on the surface of various compounds [9–12], then it becomes possible to significantly increase the radiation stability of such compounds.

SiO_2 powders have a large band gap [13], therefore, they do not absorb the main part of the solar spectrum and are prone to form protective layers on the surface of inorganic compounds [14]. ZnO powders with a certain particle size distribution show a high reflectance in solar spectrum and sufficient radiation stability when exposed to charged particles and solar spectrum quanta [15–19]. They can be used in the design of highly reflective pigments that can demonstrate stability under ionizing radiation. Therefore, ZnO and SiO_2 powders might appear to be the most suitable components for designing pigments for OSR TCCs.

In view of the above, the purpose of this work was to develop a technology for the synthesis of pigments based on ZnO and SiO_2 powders to be applied in TCCs with ultra-low α_s values.

Materials and Methods

Zn_2SiO_4 powders were synthesized by solid-state method from ZnO micropowder of PA grade (pure for analysis: average particle size 1.3 μm; weight percent of the active ingredient not less than 99.67 %) and silicon dioxide nanopowders of two brands: Aerosil A-300 (particle size of 5–20 nm, specific surface area of 300 m^2/g) and Plasmotherm (particle size of 10–12 nm, specific surface area of 180-220 m^2/g). The ratio of zinc oxide and silica powders was selected to vary from 1:0.35 to 1:0.5. To obtain zinc orthosilicate, ZnO micropowder was mixed with SiO_2 ($nSiO_2$) nanopowder in a ceramic mortar for 20 min. Next, the resulting mixture was heated in a muffle furnace at a temperature of 1100 °C for 2 h. After cooling, the obtained Zn_2SiO_4 powder was ground in a ceramic mortar for 10 min.

X-ray diffraction (XRD) spectra of the powders obtained from $ZnO + nSiO_2$ components were recorded for all their concentration ratios using Shimadzu XRD-6100 X-ray diffractometer. The diffuse reflectance spectra (ρ_λ) were recorded via Shimadzu UV-3600 Plus spectrophotometer with ISR-603 diffuse reflectance attachment within 0.2 to 2.5 μm. Solar absorptance was calculated from ρ_λ spectra using international standards [4,5] and Johnson tables [20].

Results and Discussion

The XRD spectra of Zn_2SiO_4 micropowders (Fig. 1) showed the peaks assigned to willemite – a Zn_2SiO_4 compound in its crystalline modification [21,22]. This modification was in trigonal syngony [23] with space group R-3 [24]. Additionally, the peaks were observed that could be assigned to ZnO crystalline structure in cubic phase [25].

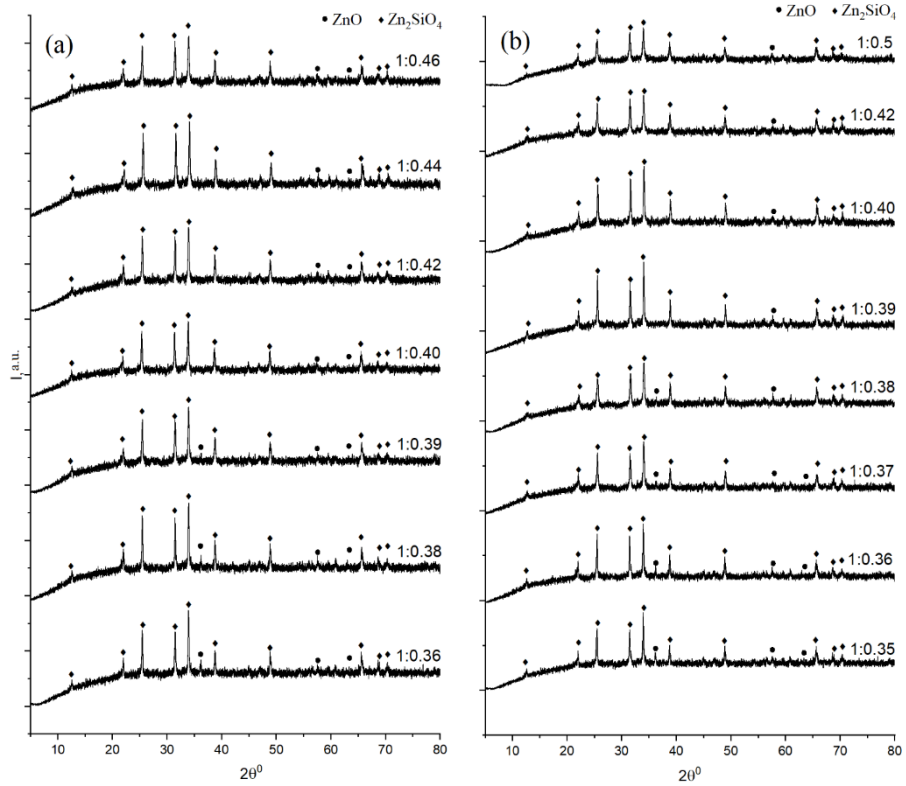

Fig. 1. XRD spectra of Zn_2SiO_4 powders obtained at different concentrations of Plasmotherm (a) and Aerosil (b) SiO_2 brands

Figure 1 demonstrates that the intensity of peaks assigned to willemite increases whereas the intensity of peaks of cubic ZnO decreases with an increase in the concentration of SiO_2 nanopowder (regardless of SiO_2 nanopowder brand). Thus, increasing the amount of the initial SiO_2 nanopowder during synthesis leads to an increase in the concentration of the target compound (willemite).

The diffuse reflection spectra of the powders used in the synthesis (Fig. 2) confirmed that the main absorption edge of the ZnO micropowder was 375 nm, which was consistent with the known values obtained by various authors [26–28]. In the longer wavelength

region, the reflectance increased and reached 93 % at $\lambda \sim 500$ nm. Within $\lambda \geqslant 1000$ nm, it gradually decreased and reached 75 % at $\lambda = 2500$ nm. The bands appeared in the spectrum at 1400, 1740, and 2240 nm, due to the absorption of OH groups sorbed on the powder surface [29–32].

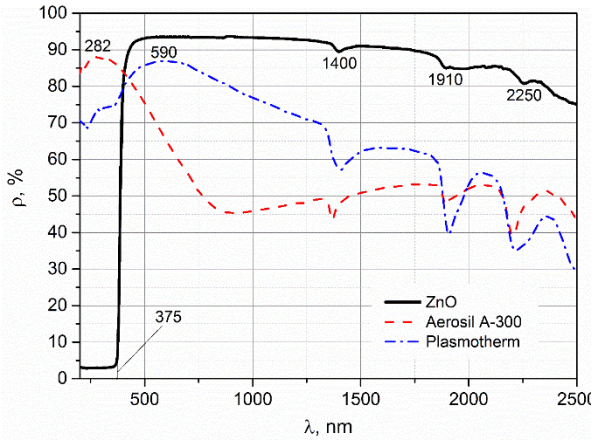

Fig. 2. The diffuse reflectance spectra for ZnO micropowder, Aerosil A-300 nanopowder, and Plasmotherm nanopowder

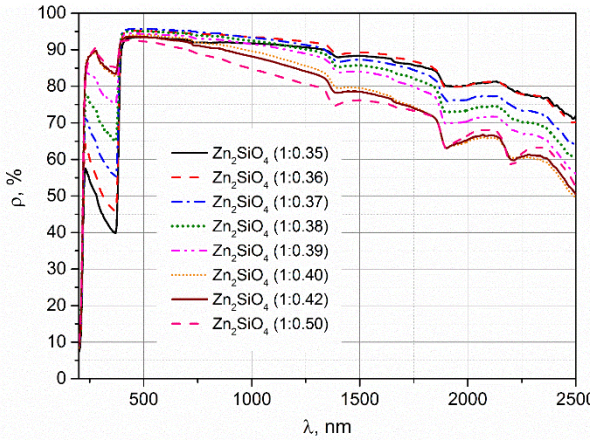

Fig. 3. The diffuse reflectance spectra for Zn_2SiO_4 powders obtained at different concentrations of Aerosil A-300 SiO_2 nanopowder

The ρ_λ spectra of SiO_2 nanopowders of Aerosil A-300 and Plasmotherm brands were characterized by a large band gap, therefore, their main absorption edge was within $\lambda < 200$ nm. The highest value of reflectance for Aerosil A-300 powder was assigned to 282 nm and reached 88 %. It decreased with an increase in the wavelength and reached the lowest value (45 %) at $\lambda = 900$ nm. In the longer wavelength region, the reflectance coefficient slightly increased, while the absorption bands of the OH groups were recorded at 1380, 1910 and 2220 nm similar to the reflectance spectrum of ZnO powder. However, the intensity of these bands for Aerosil A-300 powder was significantly higher.

The ρ_λ spectrum for SiO_2 nanopowder of Plasmotherm brand was different from the one for Aerosil A-300 by the following features: the highest value of reflectance was assigned to 590 nm, that is, it was shifted to the long-wave region; the reflectance coefficient in the longer wavelength region decreased and reached only 30 % at $\lambda = 2500$ nm. Identical absorption bands of OH groups were recorded in the reflectance spectrum of this powder, however, they displayed a much higher intensity.

The reflectance spectra of the obtained Zn_2SiO_4 powders were characterized by the following features. The main absorption edge was clearly visible for ZnO powder at the same wavelength as for the initial powder spectrum (375 nm). The highest value of reflectance was achieved at a slightly lower wavelength (410–430 nm) in comparison with the initial ZnO powder (500 nm). The reflectance coefficient gradually decreased after the highest value and up to 2500 nm. Its lowest value was consistent with the concentration of SiO_2 nanopowder during synthesis: the higher the powder concentration, the lower the reflectance coefficient.

Distinct patterns were traced in the shorter wavelength region from the main absorption edge of ZnO powder ($\lambda = 375$ nm). These patterns were presumably caused by the contribution of SiO_2 nanopowder to the reflectance spectrum of the obtained

compound Zn_2SiO_4. The reflectance increased with a decrease in the wavelength from the main absorption edge of the ZnO powder, reached the highest value, and then decreased. The highest value of reflectance increased with an increase in the concentration of SiO_2 nanopowder, i.e., the reflection spectrum peaked in the short-wave region. For Zn_2SiO_4 powder obtained using Aerosil A-300 nanopowder (Fig. 3), the absolute value of the reflectance was 57, 66, 71, 78, 83, 88, and 88% at the ratio of zinc oxide and silicon dioxide nanopowder concentrations of 1:0.35, 1:0.36, 1:0.37, 1:0.38, 1:0.39, 1:0.40, 1:0.42, 1:0.50, respectively.

The diffuse reflectance spectra of Zn_2SiO_4 powders obtained at different concentrations of Plasmotherm SiO_2 nanopowder (Fig. 4) were qualitatively the same as those for the powders obtained at different concentrations of Aerosil A-300 SiO_2 nanopowder brand (Fig. 2).

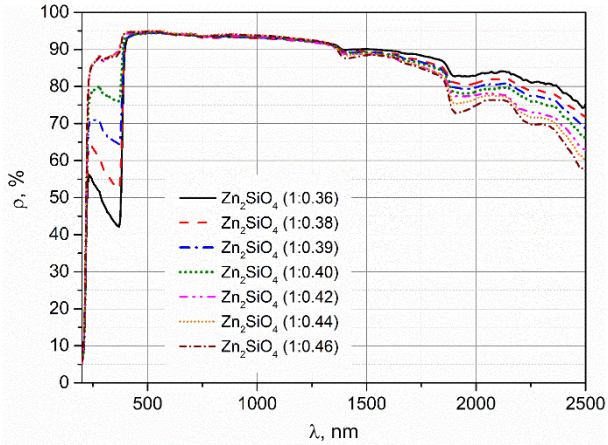

Fig. 4. The diffuse reflectance spectra of Zn_2SiO_4 powders obtained at different concentrations of Plasmotherm SiO_2 nanopowder

The absolute values of the reflectance coefficient in different regions of the spectrum were consistent with the concentration of SiO_2 nanopowder during synthesis. They were slightly different from each other and from their respective values in the spectra of Zn_2SiO_4 powders synthesized using Aerosil A-300 nanopowder. Therefore, it can be concluded that the synthesis of Zn_2SiO_4 powders obtained on the basis of ZnO micropowder and SiO_2 nanopowders of Plasmotherm and Aerosil A-300 brands at different concentrations allowed the authors to obtain pigments with high reflectance in the solar spectrum, depending on both the type of SiO_2 nanopowder and on its concentration. Because solar absorptance is the performance characteristic of TCCs,

Table 1. The correlation between α_s of Zn_2SiO_4 powders and the concentration of SiO_2 nanopowder of Aerosil A-300 brand

ZnO:nSiO_2	1:0.35	1:0.36	1:0.37	1:0.38	1:0.39	1:0.40	1:0.42	1:0.50
α_s	0.120	0.100	0.095	0.098	0.101	0.113	0.120	0.133

Table 2. The correlation between α_s of Zn_2SiO_4 powders and the concentration of SiO_2 nanopowder of Plasmotherm brand

ZnO:nSiO_2	1:0.36	1:0.38	1:0.39	1:0.40	1:0.42	1:0.44	1:0.46
α_s	0.105	0.101	0.094	0.086	0.079	0.077	0.080

it was calculated in relation to the type and concentration of SiO_2 nanopowders used during synthesis. Tables 1 and 2 contain the results of the calculations performed.

Tables 1 and 2 show that an increase in the concentration of SiO_2 nanopowders led to an increase in the absorption coefficient of the two powders obtained. The increase occurred with the lowest α_s values of 0.095 at 1:0.37 for Aerosil A-300 powder and 0.077 at 1:0.44 for Plasmotherm powder. The correlation between α_s and the concentration of SiO_2 nanopowders (Fig. 5) confirmed that the use of Plasmotherm nanopowder made it possible to synthesize Zn_2SiO_4 powders with significantly lower α_s values.

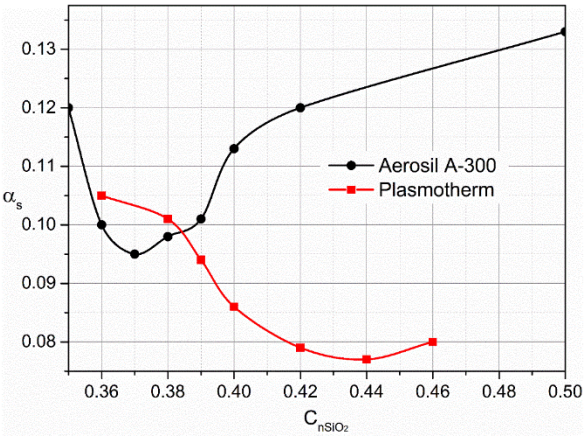

Fig. 5. The correlation between the solar absorptance (α_s) of Zn_2SiO_4 powders obtained and the concentration and type of $nSiO_2$ powders used

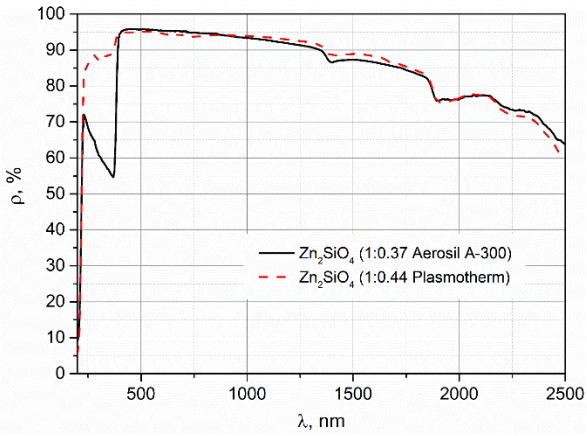

Fig. 6. Diffuse reflectance spectra of Zn_2SiO_4 powders with the lowest α_s values obtained via different types of $nSiO_2$ powder

This difference in α_s values of Zn_2SiO_4 powders was determined by the short-wave region of the diffuse reflectance spectra (Fig. 6). In this region (located at the main absorption edge of ZnO within 375 nm up to 200 nm), the reflectance coefficient of Zn_2SiO_4 powders obtained using Plasmotherm nanopowder was higher compared to the ones obtained using Aerosil nanopowder.

Conclusion

The hypothesis of the present work was that zinc oxide and silica powders could serve as the ideal starting materials for the synthesis of novel pigments to be used in thermal control coatings. Zinc oxide powders have been used as pigments for optical solar reflectors since 1960s both in Russia and in the United States who were managing their own full-scale space programs back then. These powders manifested sufficient radiation stability. Their disadvantage, however, was the large value of absorptance in the initial state ($\alpha_s \sim 0.2$) determined by the semiconductor properties and the main absorption edge. In the short-wave region from the main absorption edge ($\lambda \leqslant 375$ nm), ZnO powders absorbed 94.7 % of the energy from the radiation power of the entire solar spectrum, which is equal to 0.139 $W \cdot cm^{-2}$ [33].

If synthesis is carried out using a ZnO powder with a dielectric powder with a large band gap (e.g., SiO_2 powder), one can obtain a compound that would show a significantly lower absorptance of solar spectrum in the UV region. This work has shown that it is possible to synthesize Zn_2SiO_4 powders with high reflectance and a small value of the

solar absorptance using zinc oxide micropowders and silicon dioxide nanopowders via solid-state method. The solar absoprtance of these powders would be almost 3 times less compared to ZnO powders (α_s = 0.2 and α_s = 0.077, respectively).

Further research will be focused on the study of photo- and radiation stability of the powders obtained. The composition of Zn_2SiO_4 powders allowed the authors to assume that they would demonstrate high radiation stability when exposed to ionizing radiation. The assumption can be grounded on the following factors. The powder contains a simple $nSiO_2$ anion (i.e., not of complex composition). Such anion is unable to decompose into parts under irradiation. Therefore, no additional absorption centers might appear, as was established for complex anions of SO_4^{2-} type in $BaSO_4$ [34,35] powders or CO_3^{2-} anions in $CaCO_3$ [36] powders. If the concentration of $nSiO_2$ allows for forming its monolayer or several layers the surface of grains and granules, then these layers might act: as absorbing layers with high radiation stability [37]; as small-size defects being the relaxation centers for the primary photo- and radiation defects [38].

CRediT authorship contribution statement

Mikhail M. Mikhailov: supervision, conceptualization, writing – original draft, writing – review & editing; **Alexey V. Filimonov**: supervision, writing – review & editing; **Alexey N. Lapin**: data curation, investigation, writing – original draft; **Semyon A. Yuryev:** writing – review & editing, validation; **Vladimir A. Goronchko**: writing – review & editing, visualization; **Dmitriy S. Phedosov:** investigation, visualization.

Conflict of interest

The authors declare that they have no conflict of interest.

References

1. Zhang M, Liu C, Hu R, Hua Y, Yang Z, Wu Q, Guo L. Study on Passive-Active Cooperative Thermal Control Technology for Space Manipulator End Effectors: Design, Simulation, Testing, and On-Orbit Validation. *Case Studies in Thermal Engineering.* 2025;74: 106747.
2. Singh L, Qiu E, Cardin AE, Chen A, Luk TS, Schuller JA, Azad AK. Passive radiative thermal management using phase-change metasurfaces. *Journal of Physics: Photonics.* 2025;7(2): 025028.
3. Anderson L, Swenson C, Mattos B, Fish C, Nunes M, Wright R. Enabling the next generation of advanced small satellites through active thermal control. *Proc. SPIE 13546, Small Satellites Systems and Services Symposium (4S 2024).* SPIE; 2025. p.135462P.
4. ASTM International. *ASTM E490-22 Standard Solar Constant and Zero Air Mass Solar Spectral Irradiance Tables.* ASTM; 2022.
5. ASTM International. *ASTM E903-20 Standard Test Method for Solar Absorptance, Reflectance, and Transmittance of Materials Using Integrating Spheres.* ASTM; 2020.
6. Mikhailov MM, Lapin AN, Sokolovskiy AN, Neshchimenko VV, Yuryev SA. Optical Properties and Photostability of Microsized TiO_2 Powders Modified with its Own Nano-and Hollow Particles. *The Journal of the Astronautical Sciences.* 2023;70(5): 32.
7. Mikhailov MM, Yuryev SA, Lapin AN, Koroleva EY, Goronchko VA. Optical properties of degradation of wollastonite powders under the electron irradiation in vacuum. *Optical Materials.* 2021;119: 111342.
8. Mikhailov MM, Yuryev SA, Lapin AN, Goronchko VA, Mikhailova OA. Optical properties of aluminum oxide powder modified by nanoparticles and prospects for its use in solar power and space industry. *Acta Astronautica.* 2023;212: 483–491.

9. Huseien GF. Potential applications of core-shell nanoparticles in construction industry revisited. *Applied Nano.* 2023;4(2): 75–114.
10. Strapolova VN, Yurtov EV, Muradova AG, Sharapaev AI. Effect of magnetite nanoparticles' modification on optical properties of solar absorber coatings. *Journal of Spacecraft and Rockets.* 2018;55(1): 49–53.
11. Pavlenko VI, Cherkashina NI. Effect of SiO_2 crystal structure on the stability of polymer composites exposed to vacuum ultraviolet radiation. *Acta Astronautica.* 2019;155: 1–9.
12. Bo Z, Gang L, Kangli C, Weimin C. Preparation and space environmental stability of a nano-materials modified thermal control coating. In: Kleiman J. (ed.) *Protection of Materials and Structures from the Space Environment. Astrophysics and Space Science Proceedings, vol 47.* Cham: Springer: 2017. p.433–441.
13. Feng Q, Li B, Xiang X, Deng H, Yang G, Li S, Zu X. Ripple structure and electronic property degradation of Graphene/α-SiO_2 induced by low-Energy self-Ion irradiation. *Computational Materials Science.* 2025;246: 113347.
14. Dworak DP, Soucek MD. Protective space coatings: a ceramer approach for nanoscale materials. *Progress in Organic Coatings.* 2003;47(3–4): 448–457.
15. Kiomarsipour N, Razavi RS, Ghani K. Improvement of spacecraft white thermal control coatings using the new synthesized Zn-MCM-41 pigment. *Dyes and Pigments.* 2013;96(2): 403–406.
16. Rasmidi R, Duinong M, Chee FP. Radiation damage effects on zinc oxide (ZnO) based semiconductor devices–a review. *Radiation Physics and Chemistry.* 2021;184: 109455.
17. Khan M, Alam MS, Ahmed SF. Effect of nickel incorporation on structural and optical properties of zinc oxide thin films deposited by RF/DC sputtering technique. *Materials Physics and Mechanics.* 2023;51(1): 19–32.
18. Torres M, Franco-Urquiza EA, González-García P, Bárcena-Balderas J, Piedra S, Madera-Santana T, Quintana-Owen P. Characterization of epoxy-nanoparticle composites exposed to gamma & UV radiation for aerospace applications. *Nano Hybrids and Composites.* 2019;27: 53–65.
19. Rackauskas S, Talka T, Kauppinen EI, Nasibulin AG. Zinc Oxide Tetrapod Synthesis and Application for UV Sensors. *Materials Physics and Mechanics.* 2012;13(2): 175–180.
20. Johnson FS. The solar constant. *Journal of Atmospheric Sciences.* 1954;11(6): 431–439.
21. Jarý V, Vařák P, Babin V, Hrabovský J, Michalcova A, Volf J, Mrázek J. Scintillation properties of zinc-silicate glass-ceramics based on Zn2SiO4 willemite phase. *Optical Materials.* 2025;162: 116961.
22. Das A, Zając M, Huang WH, Chen CL, Kandasami A, Bittencourt C. The impact of willemite Zn_2SiO_4 phase in B1 to B2 type structural phase transformation in $Cd_xZn_{1-x}O$ composite thin films. *Thin Solid Films.* 2025;812: 140616.
23. Radha A, Wang SF. Influence of ZnB4O7 as an additive on the sintering temperature and microwave dielectric behaviors of Mg_2SiO_4 ceramics. *Ceramics International.* 2025;51(23): 39285–39295.
24. Syahnur FR, Permana MD, Dwiyanti D, Eddy DR, Deawati Y, Takei T, Firdaus ML. Influence of Zn2+ amount on zinc silicate phase from natural silica via hydrothermal synthesis method and evaluation of photocatalytic activity. *Emergent Materials.* 2025;8: 4423–4434.
25. Sokolov PS, Baranov AN, Dobrokhotov ZV, Solozhenko VL. Synthesis and thermal stability of cubic ZnO in the salt nanocomposites. *Russian Chemical Bulletin.* 2010;59(2): 325–328.
26. Secor JA. *Ultrafast Spectroscopy and Energy Transfer in an Organic/Inorganic Composite of Zinc Oxide and Graphite Oxide*. City University of New York; 2016.
27. Ayed S, Belgacem RB, Zayani JO, Matoussi A. Structural and optical properties of ZnO/TiO2 composites. *Superlattices and Microstructures.* 2016;91: 118–128.
28. Mikhailov MM, Lapin AN, Yuryev SA, Goronchko VA. Optical Properties of ZnO Powders Modified with ZnO Nanoparticles. *Russian Physics Journal.* 2022;65(8): 1239–1245.
29. Wilson RH, Nadeau KP, Jaworski FB, Tromberg BJ, Durkin AJ. Review of short-wave infrared spectroscopy and imaging methods for biological tissue characterization. *Journal of Biomedical Optics.* 2015;20(3): 030901.
30. Peng L, Qisui W, Xi L, Chaocan Z. Investigation of the states of water and OH groups on the surface of silica. *Colloids and Surfaces A: Physicochemical and Engineering Aspects.* 2009;334(1–3): 112–115.
31. Zhao D, Chen C, Wang Y, Ji H, Ma W, Zang L, Zhao J. Surface modification of TiO_2 by phosphate: effect on photocatalytic activity and mechanism implication. *The Journal of Physical Chemistry C.* 2008;112(15): 5993–6001.
32. Di Paola A, Bellardita M, Palmisano L, Barbieriková Z, Brezová V. Influence of crystallinity and OH surface density on the photocatalytic activity of TiO_2 powders. *Journal of Photochemistry and Photobiology A: Chemistry.* 2014;273: 59–67.
33. Makarova EA, Kharitonov AV. *Distribution of energy in the spectrum of the Sun and the solar constant*. Moscow: Nauka; 1972. (In Russian)

34. Mikhailov MM, Yuryev SA, Lapin AN. Examining the diffuse reflectance spectra and the radiation stability for the mixtures of $BaSO_4$ micropowders and SiO_2 nanopowders with various specific surface area. *Key Engineering Materials.* 2019;806: 106–112.
35. Sifontes ÁB, Cañizales E, Toro-Mendoza J, Ávila E, Hernández P, Delgado BA, Cruz-Barrios E. Obtaining highly crystalline barium sulphate nanoparticles via chemical precipitation and quenching in absence of polymer stabilizers. *Journal of Nanomaterials.* 2015;2015(1): 510376.
36. Ghadami Jadval Ghadam A, Idrees M. Characterization of $CaCO_3$ nanoparticles synthesized by reverse microemulsion technique in different concentrations of surfactants. *Iranian Journal of Chemistry and Chemical Engineering (IJCCE).* 2013;32(3): 27–35.
37. Ding W, Cheng J, Zhao L, Wang Z, Yang H, Liu Z, Chen M. Determination of intrinsic defects of functional KDP crystals with flawed surfaces and their effect on the optical properties. *Nanoscale.* 2022;14(28): 10041–10050.
38. Pastor E, Sachs M, Selim S, Durrant JR, Bakulin AA, Walsh A. Electronic defects in metal oxide photocatalysts. *Nature Reviews Materials.* 2022;7(7): 503–521.